Structural, Electronic, Elastic and Hydrogen Storage Properties of Calcium Bis(tetrahydridoborate): A First-Principles Study

S. Berri* and N. Bouarissa

Faculty of Science, University of M'sila, 28000 M'sila, Algeria

Received: 20.05.2024 & Accepted: 23.07.2024

Doi: 10.12693/APhysPolA.146.270 *e-mail: berrisaadi12@yahoo.fr

First-principles calculations were carried out to study the electronic structure and mechanical and hydrogen storage properties of calcium bis(tetrahydridoborate) using density functional theory. The obtained equilibrium lattice parameters are in good agreement with the available experimental data. The stability of the structure at zero pressure is determined by the calculation of the elastic coefficients. Nevertheless, the existence of elastic anisotropy in the compound demonstrates its lower compressibility along the c-axis than the a- and b-axes. $F2dd$-$Ca(BH_4)_2$ is nonmetallic with a wide band gap of 5.54 eV. In this regard, $Ca(BH_4)_2$ is promising for hydrogen storage applications at the expense of its high hydrogen volume density of 130 g/L (more than that of liquid hydrogen) and a hydrogen gravimetric density of 11.46 wt%, exceeding the U.S. Department of Energy's 2025 goal of 5.5 wt%.

topics: calcium bis(tetrahydridoborate), density functional theory (DFT), hydrogen storage

1. Introduction

Over the past decades, different energy storage methods have been investigated for different materials belonging to different compound groups [1–5]. There are various ways to save energy, from superconductivity to supercapacitance, through the use of thermoelectric, photocatalytic, and photovoltaic materials. Moreover, finding an inexpensive and environmentally friendly procedure to fabricate devices that enable energy storage to the greatest possible extent for various applications is the focus of attention of many material science researchers [6–15].

Thermoelectric materials and devices have undergone considerable development in recent decades [16–18]. Despite extensive studies, current state-of-the-art thermoelectric studies are not viable for large-scale commercial applications due to their low efficiency or reliance on rare or hazardous materials like lead and tellurium [17–21]. Additionally, materials with excellent optical properties and high absorption rates have potential applications in the field of renewable energy since they can serve as absorbers in photovoltaic (PV) devices. Silicon (Si) is commonly used as a photovoltaic absorber due to its abundance, cost-effectiveness, and potential for application in advanced processing technologies [22].

Hydrides are the most important structures that can be used for hydrogen storage [23–26]. The archetypical example, i.e., calcium bis(tetrahydridoborate) ($Ca(BH_4)_2$) decomposes (and reabsorbs) hydrogen along three possible decomposition pathways, which are described in [27–29] as follows

$$Ca(BH_4)_2 \longleftrightarrow \tfrac{2}{3}\ CaH_2 + \tfrac{1}{3}\ CaB_6 + \tfrac{10}{3}\ H_2 \quad (1)$$

(with 9.6 wt% of H_2 and ΔH=32 kJ/mol),

$$Ca(BH_4)_2 \longleftrightarrow CaH_2 + 2\ B + 3\ H_2 \quad (2)$$

(with 8.7 wt% of H_2 and ΔH=56 kJ/mol),

$$Ca(BH_4)_2 \longleftrightarrow \tfrac{1}{6}\ CaB_{12}H_{12} + \tfrac{5}{6}\ CaH_2 + \tfrac{13}{6}\ H_2 \quad (3)$$

(with 6.3 wt% of H_2 and ΔH=34–36 kJ/mol).

The enthalpy of reactions (1)–(3) is obtained by density functional theory (DFT) calculations [27–29].

Experimentally, about 9.0 mass % of hydrogen was released when $Ca(BH_4)_2$ was heated to 800 K [30, 31]. Simone Di Cataldo et al. [32] investigated $Ca(BH_4)_2$, and their study shows that the direct band gap is 5 eV for the given material. Research on doped metal borohydrides suggests high-temperature superconductivity, with critical temperatures up to 110 K [32]. Our motivation to study this material comes from the fact that it has already been synthesized among the light

metal borohydrides $M(BH_4)_n$ (M = Li, Na, Mg, Ca). These compounds present interesting properties, particularly in terms of hydrogen storage capacity, but also yield promising results pointing towards the possibility of reversibility during successive A/D cycles. With a high storage capacity of about 10 wt% (actually achievable under experimental conditions) and a relatively low dehydrogenation temperature, $Ca(BH_4)_2$ shows promise as a viable and reversible hydrogen storage material under appropriate conditions [33]. Inspired by these interesting results, the present study focuses on exploring the electronic structure, mechanics, and hydrogen storage properties of $Ca(BH_4)_2$. The details of the calculation will be introduced in the next section. Additionally, the electronic band structure behavior, mechanics, desorption temperature, and volumetric and gravimetric hydrogen storage will be analyzed in detail.

TABLE I

The relationship between the Lagrangian deformation and the corresponding coefficient.

Strain type	Sumary of elastic constants
$A_1 = (\gamma, 0, 0, 0, 0, 0)$	C_{11}
$A_2 = (0, \gamma, 0, 0, 0, 0)$	C_{12}
$A_3 = (0, 0, \gamma, 0, 0, 0)$	C_{33}
$A_4 = (\gamma, \gamma, 0, 0, 0, 0)$	$C_{11} + C_{22} + 2C_{12}$
$A_5 = (\gamma, 0, \gamma, 0, 0, 0)$	$C_{11} + C_{33} + 2C_{13}$
$A_6 = (0, \gamma, \gamma, 0, 0, 0)$	$C_{22} + C_{33} + 2C_{23}$
$A_7 = (\gamma, 0, 0, 2\gamma, 0, 0)$	$C_{11} + 4C_{44}$
$A_8 = (\gamma, 0, 0, 0, 2\gamma, 0)$	$C_{11} + 4C_{55}$
$A_9 = (\gamma, 0, 0, 0, 0, 2\gamma)$	$C_{11} + 4C_{66}$

2. Computational method

The present study used the CASTEP package [34] with projector-augmented wave potential and density functional theory (DFT) approach based on the plane wave pseudo-potential method to perform *ab initio* calculations. The Perdew–Burke–Ernzerhof (PBE) potential [35] was used to manage the correlation of electronic exchanges. The energy cutoff was set at 520 eV to determine the structural, electronic, magnetic, and elastic properties of the $Ca(BH_4)_2$ phase. The conjugate gradient method was used to optimize the ionic positions, with the structural parameters obtained through Hellmann–Feynman forces showing energy convergence below 0.001 eV/Å within a criterion of 10^{-7} eV. The Brillouin zone was modeled using a $15 \times 15 \times 3$ Monkhorst–Pack [36] grid, and Brillouin-zone integrations were performed via the Methfessel–Paxton [37] smearing method with a smearing parameter of 0.1 eV.

We used the strain energy–strain curve to calculate the elastic constants. For $Ca(BH_4)_2$ with orthorhombic structure, there are nine independent elastic constants: C_{11}, C_{12}, C_{13}, C_{22}, C_{23}, C_{33}, C_{44}, C_{55}, and C_{66}. To calculate the full elastic constants, the nine Lagrangian strain tensors in terms of a parameter γ are listed in Table I.

For each strain, γ varied between -0.02 and 0.02 with a step of 0.002, i.e., we had to calculate the total strain energies of 21 points for each strain tensor. The calculated E–γ points were then fitted to the least-squares polynomial, and the elastic constants could be inferred from the second-order derivatives of E with respect to γ. Details of the calculations were introduced in [38]. Based on the Voigt–Reuss–Hill approximation, other mechanical parameters for polycrystalline aggregates, such as bulk modulus B, shear modulus G, Poisson's ratio ν, and the Vickers hardness H_V, can be obtained via elastic constants. According to the Voigt and Reuss approximation, the bulk modulus and the shear modulus for orthorhombic crystals can be written in the form [39]

$$B_V = \frac{1}{9}(C_{11}+C_{12}+C_{33}+2C_{12}+2C_{13}+2C_{23}), \quad (4)$$

$$B_R = \phi\Big[C_{11}(C_{22}+C_{33}-2C_{23})+C_{22}(C_{33}-2C_{13}) -2C_{33}C_{12}+C_{12}(2C_{23}-C_{12}) +C_{13}(2C_{12}-C_{13}) + C_{23}(2C_{13}-C_{23})\Big]^{-1}, \quad (5)$$

$$G_R = 15\left\{3\left(\frac{1}{C_{44}}+\frac{1}{C_{55}}+\frac{1}{C_{66}}\right) +\frac{4}{\phi}\Big[C_{11}\big(C_{22}+C_{33}+C_{23}\big) +C_{22}\Big(C_{33}+C_{13}+C_{33}C_{12}-C_{12}(C_{23}+C_{12}) +C_{13}(C_{12}+C_{13})-C_{23}(C_{13}+C_{23})\Big)\Big]\right\}^{-1}, \quad (6)$$

with

$$\phi = C_{12}(C_{12}C_{13}-C_{13}C_{22}) + C_{23}(C_{13}C_{12}-C_{23}C_{11}) +C_{33}(C_{11}C_{22}-C_{12}^2), \quad (7)$$

$$\frac{1}{G_V} = \frac{1}{15}\Big[5(C_{11}+C_{22}+C_{33}) - (C_{12}+C_{12}+C_{23}) +\frac{3}{15}(C_{44}+C_{55}+C_{66})\Big], \quad (8)$$

$$G_H = \frac{1}{2}(G_V + G_R), \quad (9)$$

$$B_H = \frac{1}{2}(B_V + B_R), \quad (10)$$

$$E = \frac{9B_H G_H}{3B_H + G_H}, \tag{11}$$

$$\nu = \frac{3B_H - 2G_H}{2(3B_H + G_H)}, \tag{12}$$

$$A_z = \frac{G_V - G_R}{G_V + G_R}. \tag{13}$$

The results are discussed and compared in terms of their suitability for use in hydrogen storage and other applications.

3. Results and discussion

3.1. Structural properties

$Ca(BH_4)_2$ crystallizes in an orthorhombic system with the space group ($F2dd$). The results of X-ray diffraction (XRD) experiments revealed that $Ca(BH_4)_2$ is a structure (see Fig. 1) with Ca, B, and H atoms occupying the atomic positions (see Table II).

Table III lists the calculated structural properties of $Ca(BH_4)_2$, along with other experimental and theoretical data. The compound $Ca(BH_4)_2$ has structural parameter values of $a = 8.7068$ Å, $b = 13.1080$ Å, and $c = 7.6815$ Å. These values closely match theoretical results reported in previous studies [30, 40]. The optimized structures are quite reliable because the deviation between the theoretically predicted lattice parameters and those measured experimentally [30, 41–43] is less than 0.2 Å.

3.2. Elastic properties

The elastic constants C_{ij}, the volume modulus B, and the shear modulus G are the key parameters of the elastic properties of materials. Understanding the elastic properties of materials is useful for their industrial application. The elastic constant C_{ij} reflects the response of a material to external stress and enables the derivation of important mechanical information such as the mechanical stability, bearing capacity, and bonding characteristics of the compound. For orthorhombic crystals, the Born–Huang stability criteria $C_{ii} > 0$ ($i = 1$–6), $C_{11} + C_{22} - 2C_{12} > 0$, $C_{11} + C_{33} - 2C_{13} > 0$, $C_{22} + C_{33} - 2C_{23} > 0$, $C_{11} + C_{22} + C_{33} + 2(C_{13} + C_{13} + C_{23}) > 0$ must be reached [38]. The basic parameters of the elastic properties of $Ca(BH_4)_2$ are listed in Table IV, and they all satisfy the mechanical stability requirements. Table IV lists the elastic constants of the compound $Ca(BH_4)_2$, which were obtained at zero temperature and zero pressure. The value of elastic stiffness in response to deformations along the (001)(c-axis) and (100)(a-axis) directions is obtained from the elastic constants C_{33} and C_{11}, respectively. As C_{33} exceeds C_{11}, it follows that the c-axis compressibility is greater than the a-axis compressibility. Quantification of the elastic constant C_{12} is used to determine the elasticity present in the ⟨100⟩ direction in the (110) plane. Parameters C_{66} and C_{44} correlate with the ability to withstand shear stress in the 100 planes along the ⟨110⟩ orientation and the 010 or 100 planes along the ⟨001⟩ direction, respectively.

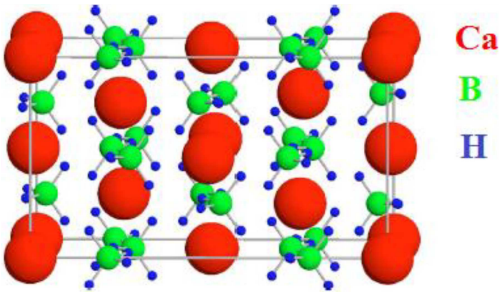

Fig. 1. Crystal structure of $Ca(BH_4)_2$ [30].

TABLE II

Atomic coordinates of $Ca(BH_4)_2$ compound [30].

Atom	x	y	z
Ca	0	0	0
B	0.0056(9)	0.2243(2)	0.0081(11)
H	0.0056(9)	0.2243(2)	0.0081(11)
H	0.0345(19)	0.1817(11)	0.1256(14)
H	−0.1180(10)	0.2553(12)	0.012(2)
H	0.0910(15)	0.2922(9)	0.028(2)

The modulus of elasticity B is a parameter that characterizes the breaking resistance of materials. The strain that changes volume without changing shape is called compression, and the strain that changes shape without changing volume is called shear. Both parameters, B and G, are used to measure the crystal's ability to resist deformation. The larger the B and G, the stronger the resistance to deformation. The mechanical resistance of compounds is represented by Young's modulus. A higher Young's modulus value indicates that the fracturing tendency of the material is more sophisticated [44]. The calculated values of all these alloy parameters are presented in Table V.

Prediction of hardness and ductility of materials can be carried out with high accuracy, with considerable support from various factors such as Pugh ratio (G/B), Poisson ratio (ν), and Cauchy pressure. These parameters play a crucial role in understanding the mechanical behavior of materials. Poisson's ratio ν provides valuable information about the ductility of a material. A material with a Poisson's ratio equal to or greater than 0.26 exhibits a ductile nature, which implies that it can undergo plastic deformation before fracture. On the other

TABLE III

Lattice constants a [Å], b [Å], and c [Å] with total energy E_{tot} [eV].

Method, work	a [Å]	b [Å]	c [Å]	E_{tot} [eV]
PBE	8.7068	13.1080	7.6815	−2572.692
Theor. [30]	8.802	13.244	7.473	–
Theor. [40]	8.745	13.105	7.495	–
Exper. [41]	8.7782(2)	13.129(1)	7.4887(9)	–
Exper. [42]	8.7759(3)	13.0234(4)	7.4132(2)	–
Exper. [43]	8.7782(2)	13.129(1)	7.4887(9)	–

TABLE IV

Calculated elastic constants C_{ij} [GPa] of $Ca(BH_4)_2$ material.

Elastic constants	$Ca(BH_4)_2$
C_{11}	27.34
C_{12}	0.31
C_{13}	10.14
C_{22}	31.09
C_{23}	−5.36
C_{33}	33.18
C_{44}	6.97
C_{55}	18.93
C_{66}	9.52

TABLE V

Calculated values of polycrystalline bulk (B), shear (G) and Young's (E) moduli, Poisson's ratio (ν), and compressibility (β) of $Ca(BH_4)_2$ compound.

Elastic constants	$Ca(BH_4)_2$
B_V [GPa]	11.30
B_R [GPa]	11.02
B_H [GPa]	11.16
G_V [GPa]	12.85
G_R [GPa]	10.85
G_H [GPa]	11.85
E_x [GPa]	24.11
E_y [GPa]	30.07
E_z [GPa]	28.45
ν_{xy}	0.06
ν_{yx}	0.08
ν_{zx}	0.37
ν_{yz}	−0.18
ν_{zy}	−0.17
ν_{xz}	0.316
A_z	0.94
β [GPa^{-1}]	0.09070

hand, materials with a Poisson's ratio lower than 0.26 are considered brittle and prone to fracture without significant deformation [38]. Another key factor in determining the ductility of a material is the G/B ratio. When the G/B ratio is less than 0.57, it means that the material has ductile properties and is capable of withstanding significant deformations under stress. Conversely, a G/B ratio greater than 0.57 suggests a brittle nature, i.e., that the material is subject to fracturing without undergoing significant deformation [44]. The Cauchy pressure is an essential parameter in this context. Positive values of the Cauchy pressure indicate a brittle nature of the material, meaning that its strength is influenced more by compression than by tension. On the other hand, negative values of Cauchy pressure imply a ductile nature, suggesting that the material's resistance to fracture is influenced more by tension than compression.

The generation of microcracks during the use of materials is closely related to elastic anisotropy and affects the service life of materials [45]. Therefore, we calculated the elastic anisotropy of $Ca(BH_4)_2$, which is usually expressed by the anisotropy index standard equation (11). If $A_z = 0$ or 1, then the material is isotropic. Otherwise, it is anisotropic.

To demonstrate elastic anisotropy in more detail, the variation of Young's modulus, compressibility, shear modulus, and Poisson's ratio in different crystallographic directions should be considered. In order to explore this anisotropic nature, we estimated the 3D and 2D plane-projected variations of G, E, ν, and B of $Ca(BH_4)_2$ using the ELATE code [46]. The defect-free circle or sphere symbolizes the quality of being isotropic, while any difference from these shapes implies anisotropy. The lower and upper limits of the aforementioned parameters are shown in Table IV (see [33, 47]). The 3D curved surfaces of G, E, ν, and β are shown, respectively, in Figs. 2–5 in panel d. The 3D elliptical surface indicates the elastic isotropy of the material (otherwise it is anisotropic). To distinguish the behavior in different planes, 2D plots in three main planes are also shown in Figs. 2–5 in panels a–c.

3.3. Electronic structure

Band structure is an important parameter in the application of semiconductors in photovoltaic and optoelectronic devices, as it affects the whole

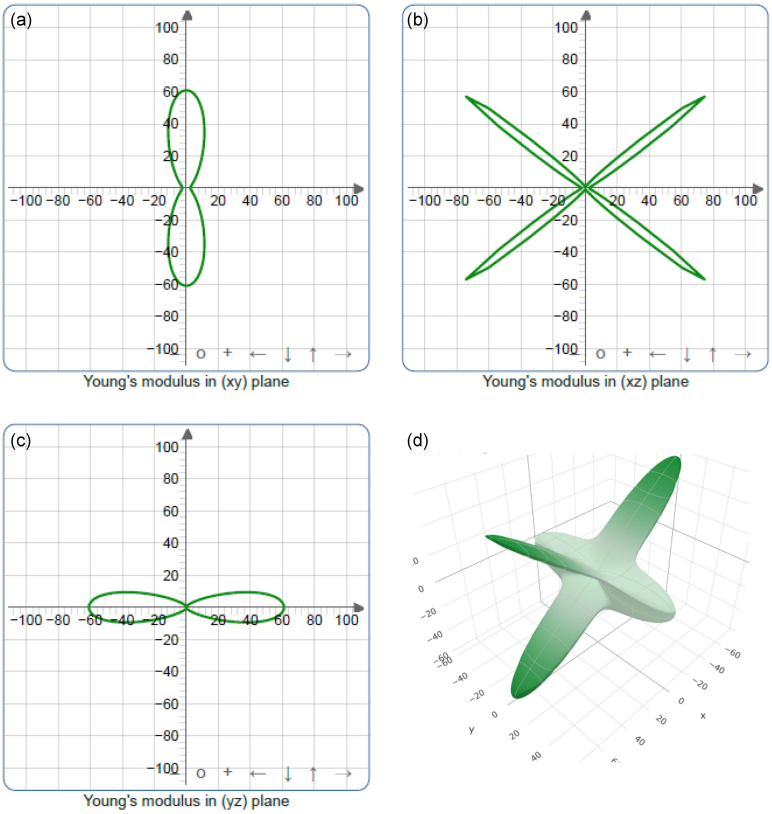

Fig. 2. The 2D and 3D plots of Young's modulus (E) of $Ca(BH_4)_2$.

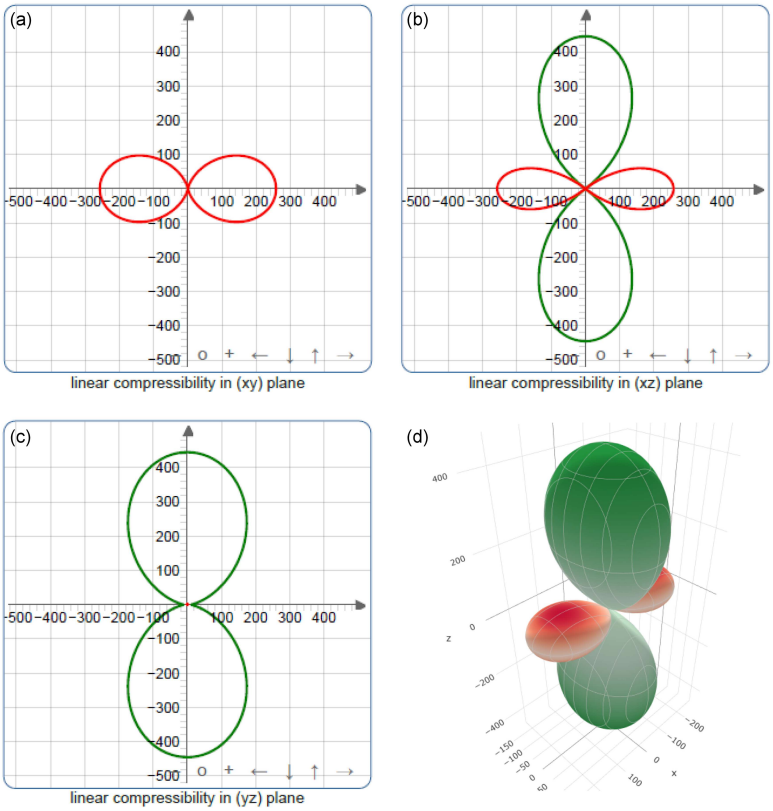

Fig. 3. The 2D and 3D plots of Poisson's ratio (ν) of $Ca(BH_4)_2$.

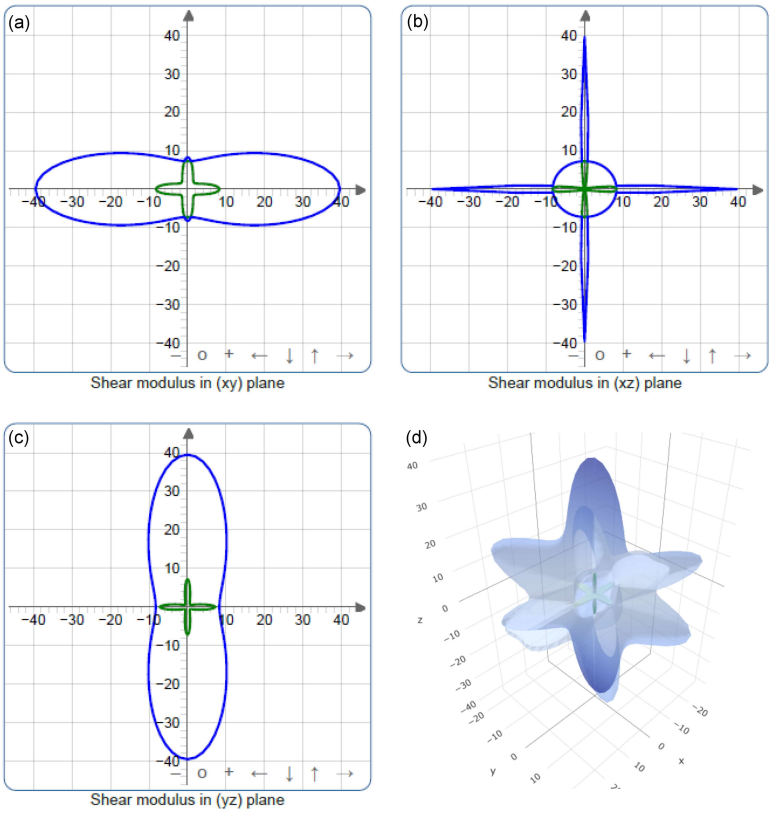

Fig. 4. The 2D and 3D plots of shear modulus (G) of $Ca(BH_4)_2$.

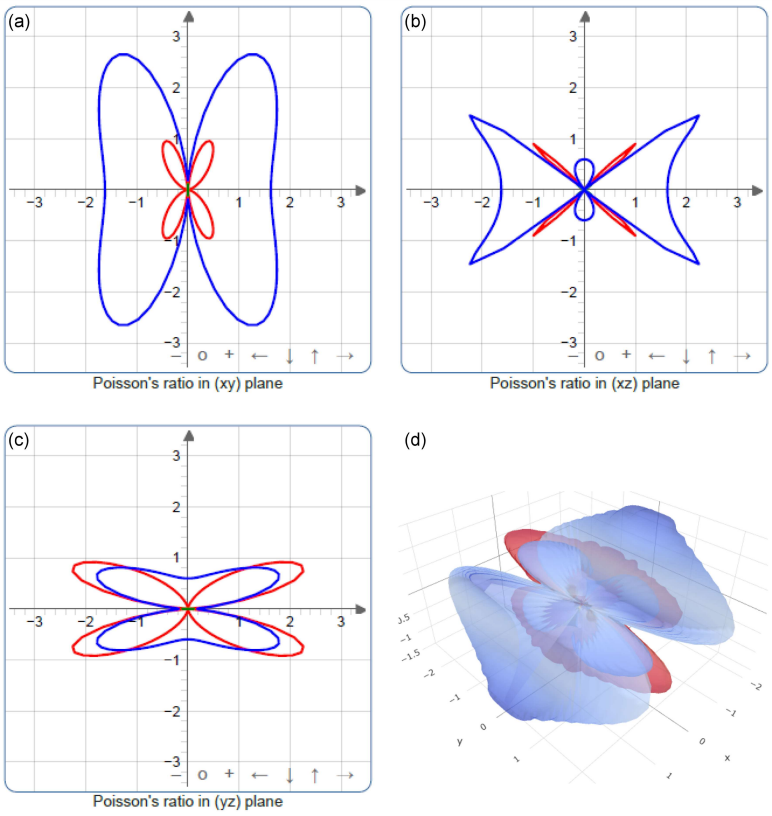

Fig. 5. The 2D and 3D plots of linear compressibility (β) of $Ca(BH_4)_2$.

TABLE VI
Energy band gap for $Ca(BH_4)_2$.

	Reference	E_g [eV]
$Ca(BH_4)_2$	This work	5.54
	[33]	5
	[47]	4.9

process of carrier generation, separation, and recombination [48, 49]. The band gap value, direct or indirect band gap, and electronic state dispersion reflect the most important information in electronics, which usually determines the physical properties of the materials under study. Therefore, the electronic band structures of $Ca(BH_4)_2$ were calculated and analyzed. The calculated band structure and total density of states for $Ca(BH_4)_2$ are shown in Fig. 6. A large energy gap of approximately 5.549 eV in Fig. 6 indicates that $Ca(BH_4)_2$ is a wide-gap insulator. We have presented our calculated band gap values in Table VI along with previously reported theoretical results because we found no experimental band structure (BS) data of $Ca(BH_4)_2$. A larger band gap generally corresponds to a higher intrinsic carrier concentration, while a smaller band gap results in a higher intrinsic carrier concentration. This relationship is due to the energy required to promote electrons from the valence band to the conduction band [50]. These materials enable the use of smaller and more efficient power electronics than their silicon-based counterparts due to their higher band gaps, melting points, and thermal conductivities [51]. The most studied classes of wide band gap semiconductors are nitrided materials (e.g., GaN), carbides (e.g., SiC), and group VI chalcogenides (Ch = O, S, Se, Te) [52]. Wide band gap (WBG) semiconductors are a broad class of materials widely used in commercially produced electronic devices, as well as in emerging energy applications, such as photovoltaic (PV) solar cells, energy separation devices, and photo-electrochemical (PEC) water-splitting devices [50–54].

3.4. Hydrogen storage properties

The gravimetric density of hydrogen is an important parameter in the search for hydrogen storage materials before studying atomic structure prediction and mechanical stability. The gravimetric density of hydrogen for $Ca(BH_4)_2$ is estimated using the following equation [55]

$$C\ [\text{wt\%}] = \frac{n\,M_{\text{H}}}{n\,M_{\text{H}} + M_{\text{com}}} \times 100\%, \tag{14}$$

where n represents the ratio between hydrogen and atoms of the material, and M_{H} and M_{com} represent the molar masses of hydrogen and the compound, respectively. The gravimetric density of hydrogen for $Ca(BH_4)_2$ compounds was calculated to

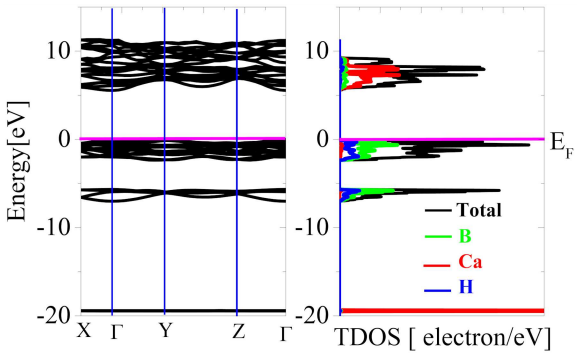

Fig. 6. The calculated electronic band structure and total density of states for $Ca(BH_4)_2$.

be 11.46 wt%, which is higher than that set by the US Department of Energy, which is 4.5 wt% for practical applications [25, 55]. Additionally, we calculated the volumetric hydrogen storage capacities (V_{sc}) of $Ca(BH_4)_2$ to better understand their hydrogen storage potential [53]. It turns out that $Ca(BH_4)_2$ has a gravimetric hydrogen density (GHD) of 11.46 wt% of H_2 and a volumetric capacity of $V_{\text{sc}} = 130$ g/L, which corresponds to the target set by the US-DOE for 2025.

The volumetric hydrogen storage capacity V_{sc} [kg H_2/m^3] is given by the following formula [56]

$$V_{\text{sc}} = \frac{m_{\text{H}_2} - m^0_{\text{H}_2}}{V}, \tag{15}$$

where m_{H_2} is the total mass of hydrogen present in the calculated volume, $m^0_{\text{H}_2}$ is the mass of hydrogen in the overall phase, and V is the effective volume. It is found that $Ca(BH_4)_2$ has the highest GHD of 11.46 wt% and the highest volumetric capacity of $V_{\text{sc}} = 130$ g/L.

In order to use hydrides for solid-state hydrogen storage purposes, thermodynamic stability is one of the imperative parameters because it influences both the amount of hydrogen that can be stored and the duration of its storage. To evaluate the thermodynamic stability of $Ca(BH_4)_2$ hydrides, we determined their formation enthalpies (ΔH), which constitute an important quantity and can be used to evaluate the thermodynamic stability of the studied hydrides.

This helps to determine the approximate temperature at which hydrogen is released from the hydride. Basically, ΔH is the measure of the energy required to form a compound with the fusion of the constituent elements. The value of ΔH is negative for hydrides because energy is released whenever hydrogen is bonded to another element. The most negative value of ΔH results in the most stable hydride. Generally, $\Delta H < 0$ indicates that the hydrides studied are stable, while $\Delta H > 0$ reveals instability. The following relationship is used to determine ΔH, which is the difference between the total energies of the products and the reactants, namely

$$\Delta H = \sum E^{tot}_{\text{product}} - \sum E^{tot}_{\text{reacant}}. \quad (16)$$

The formation of $Ca(BH_4)_2$ hydride is obtained by the following relation

$$\Delta H = E^{tot}_{Ca(BH_4)_2} - 4E^{tot}_{H_2}. \quad (17)$$

The calculated energy value of the H_2 molecule is 31.70 eV, which is equal to 31.70 eV, as reported by Abdellaoui et al. [57]. The calculated ΔH value for $Ca(BH_4)_2$ hydride is -0.355 eV/atom, which proves that $Ca(BH_4)_2$ hydride is thermodynamically stable.

The use of the standard Gibbs energy (ΔG) allows the thermodynamic properties of hydrides to be evaluated. It can be represented by the following expression [57]

$$\Delta G = \Delta H - T\,\Delta S. \quad (18)$$

Here, formation enthalpies ΔH and the entropy change ΔS of the dehydrogenation reaction are used to measure the temperature of the dehydrogenation reaction. When the material is heated, ΔS gradually prevails over ΔH, and then ΔG becomes zero at constant decomposition pressure and temperature. Thus, the dehydrogenation temperature can be evaluated by the following relationship [57, 58]

$$T_{\text{de}} = -\frac{\Delta H}{\Delta S}. \quad (19)$$

When making a comparison between gases and solids, it becomes evident that the magnitude of entropy loss ΔS for solids is much smaller. The observed discrepancy can be attributed to the increased level of disorder exhibited by gases compared to solids when exposed to thermal energy. The production of hydrogen gas (H_2) is the main factor influencing the change in entropy during the decomposition process. According to the prevailing view among scientific experts, as evidenced in the scientific literature, the entropy ΔS of the H_2 molecule is approximately -130.7 J/(mol K) when evaluated under standard temperature and pressure conditions [59]. The calculated desorption temperature for $Ca(BH_4)_2$ is 262.06 K. These calculated desorption temperature values are significantly good compared to the critical point of hydrogen (33.20 K).

4. Conclusions

In this paper, we conducted a detailed study of the structural, electronic, elastic, and hydrogen storage properties of the compound $Ca(BH_4)_2$. The relaxed unit-cell constants (a = 8.7068 Å, b = 13.1080 Å, c = 7.6815 Å) agree well with the experimental data from the PBE functional. The calculated values of the ground state lattice parameters are very close to the experimental values. Our calculated band gap values revealed that $Ca(BH_4)_2$ is a wide band gap insulating material, which is consistent with previous theoretical results. Then, the mechanical stability is determined by the elastic stiffness constants, which reveal that $Ca(BH_4)_2$ hydrides are mechanically stable because they meet the Born stability requirements. In this regard, $Ca(BH_4)_2$ has shown promise for hydrogen storage applications due to its high hydrogen volume density of 130 g/L and gravimetric hydrogen density of 11.46 wt%, which exceeds the U.S. Department of Energy's 2025 goal of 5.5 wt%.

References

[1] R.U. Amate, P.J. Morankar, A.M. Teli, S.A. Beknalkar, G.T. Chavan, N.A. Ahir, D.S. Dalavi, C. Jeon, *Chem. Eng. J.* **484**, 149556 (2024).

[2] G. Yang, X. Zhao, F. Liao, Q. Cheng, L. Mao, H. Fa, L. Chen, *Sustain. Energy Fuels* **5**, 3039 (2021).

[3] F. Shirvani, A. Shokri, B. Abedi Ravan, M.S. Akhoundi Khezrabad, *Solid State Commun.* **343**, 114642 (2022).

[4] R. Vicentini, R. Beraldo, J. Aguiar, F. Oliveira, F. Runo, D. Larrude, L. Da Silva, H. Zanin, *J. Energy Storage* **44**, 103371 (2021).

[5] F. Shirvani, A. Shokri, *Phys. B Condens. Matter* **649**, 414459 (2023).

[6] V. Laguta, M. Marysko, V. Stephanovich et al., *Acta Phys. Pol. A* **131**, 1534 (2017).

[7] K. Domieracki, D. Kaczorowski, *Acta Phys. Pol. A* **130**, 593 (2016).

[8] J. Gosk, M. Boćkowski, M. Tokarczyk, G. Kowalski, A. Twardowski, *Acta Phys. Pol. A* **124**, 877 (2013).

[9] S. Mammadova, E. Nakhmedov, O. Alekperov, *Acta Phys. Pol. A* **129**, 800 (2016).

[10] S. Berri, *Comput. Condens. Matter* **29**, e00595 (2021).

[11] S. Berri, *J. Phys. Chem. Solids* **170**, 110940 (2022).

[12] S. Berri, *Acta Phys. Pol. A* **138**, 834 (2018).

[13] S. Berri, *Chem. Phys. Lett.* **826**, 140653 (2023).

[14] S. Berri, *Chinese J. Phys.* **55**, 2476 (2017).

[15] S. Berri, *Comput. Condens. Matter.* **28**, e00586 (2021).

[16] L.E. Bell, *Science* **321**, 1457 (2008).

[17] I. Chowdhury, R. Prasher, K. Lofgreen, G. Chrysler, S. Narasimhan, R. Mahajan, D. Koester, R. Alley, R. Venkatasubramanian, *Nat. Nanotechnol.* **4**, 235 (2009).

[18] L. Shi, C. Dames, J.R. Lukes, P. Reddy, J. Duda, D.G. Cahill, J. Lee, A. Marconnet, K.E. Goodson, J.-H. Bahk, *Nanoscale Microscale Thermophys. Eng.* **19**, 127 (2015).

[19] S.R. Bull, *Proc. IEEE* **89**, 1216 (2001).

[20] M. Zhu, C. Lu, L. Liu, *Iscience* **26**, 106718 (2023).

[21] S. Berri, *Comput. Condens. Matter.* **39**, e00902 (2021).

[22] M.A. Green, *Nat. Energy* **1**, 15015 (2016).

[23] A.-L. Chaudhary, S. Dietzel, H.-W. Li et al. *Int. J. Hydrogen Energy* **42**, 11422 (2017).

[24] H.X. Li, C.B. Wan, X.C. Li et al. *Int. J. Hydrogen Energy* **47**, 1723 (2022).

[25] S. Al, M. Yortanlı, E. Mete, *Int. J. Hydrogen Energy* **45**, 18782 (2020).

[26] A. Gencer, G. Surucu, S. Al, *Int. J. Hydrogen Energy* **44**, 11930 (2019).

[27] C.B. Minella, S. Garroni, C. Pistidda et al., *J. Phys. Chem. C* **115**, 2497 (2011).

[28] T.J.J. Frankcombe, *Phys. Chem. C* **114**, 9503 (2010).

[29] V. Ozolins, E.H. Majzoub, C. Wolverton, *J. Am. Chem. Soc.* **131**, 230 (2009).

[30] K. Miwa, M. Aoki, T. Noritake, N. Ohba, Y. Nakamori, S. Towata, A. Züttel, S. Orimo, *Phys. Rev. B* **74**, 155122 (2006).

[31] J.-H Kim, S.-A. Jin, J.-H. Shim, Y.W. Cho, *J. Alloys Compd.* **461**, L20 (2008).

[32] S. Di Cataldo, L. Boeri, *Phys. Rev. B* **107**, L060501 (2023).

[33] C. Rongeat, I. Lindemann, A. Borgschulte, L. Schultz, O. Gutfleisch, *Int. J. Hydrogen Energy* **36**, 247 (2011).

[34] D. Vanderbilt, *Phys. Rev. B* **56**, 1625 (1997).

[35] J.P. Perdew, K. Burke, M. Ernzerhof, *Phys. Rev. Lett.* **77**, 3865 (1996).

[36] H.J. Monkhorst, J.D. Pack, *Phys. Rev. B* **13**, 5188 (1976).

[37] M. Methfessel, A.T. Paxton, *Phys. Rev. B* **40**, 3616 (1989).

[38] F. Mouhat, F.-X. Coudert, *Phys. Rev. B* **90**, 224104 (2014).

[39] R. Hill, *Proc. Phys. Soc. Sect. A* **65**, 349 (1952).

[40] Y.-S. Lee, Y. Kim, Y.W. Cho, D. Shapiro, C. Wolverton V. Ozoliņš, *Phys. Rev. B* **79**, 104107 (2009).

[41] C. Comanescu, *Energies* **16**, 4536 (2023).

[42] Y. Filinchuk, E. Ronnebro, D. Chandra, *Acta Mater.* **57**, 732 (2009).

[43] S. Berri, *J. Supercond. Nov. Magn.* **33**, 3809 (2020).

[44] J. Hirsch, *Acta Phys. Pol. A* **133**, 350 (2018).

[45] M.G. Brik, *J. Phys. Chem. Solid* **71**, 1435 (2010).

[46] R. Gaillac, P. Pullumbi, F.-X. Coudert, *J. Phys. Condens. Matter* **28**, 275201 (2016).

[47] M. Aoki, K. Miwa, T. Noritake, H.-W. Li S.-i. Orimo, *R&D Rev. Toyota CRDL* **44**, 43 (2013).

[48] M.D. Segall, R. Shah, C.J. Pickard, M.C. Payne, *Phys. Rev. B* **54**, 16317 (1996).

[49] B.G. Yacobi, *Semiconductor Materials: An Introduction to Basic Principles*, Springer 2003, p. 1.

[50] P.P. Altermatt, A. Schenk, F. Geelhaar, G. Heiser, *J. Appl. Phys.* **93**, 1598 (2003).

[51] J. Millán, P. Godignon, X. Perpiñà, A. Pérez-Tomás, J. Rebollo, *IEEE Trans. Power Electron.* **29**, 2155 (2014).

[52] S. Berri, *Eur. Phys. J. B* **93**, 191 (2020).

[53] W.N. Shafarman, L. Stolt, *Cu(InGa)Se$_2$ Solar Cells*, John Wiley & Sons, 2003.

[54] X. Wu, *Solar Energy* **77**, 803 (2004).

[55] H.H. Raza, G. Murtaza, Umm-e-Hani, N. Muhammad, S.M. Ramay, *Int. J. Quant. Chem.* **120**, e26419 (2020).

[56] X. Zhang, D. Cao, J. Chen, *J. Phys. Chem. B* **107**, 4942 (2003).

[57] M. Abdellaoui, M. Lakhal, H. Benzidi, M. Garara, A. Benyoussef, A. El Kenz, O. Mounkachi, M. Loulidi, H. Ez-Zahraouy, *Appl. Phys. A* **125**, 760 (2019).

[58] M. Garara, H. Benzidi, M. Abdellaoui, M. Lakhal, A. El kenz, A. Benyoussef, O. Mounkachi M. Loulidi, *Mater. Chem. Phys.* **254**, 123417 (2020).

[59] A. Mera, M.A. Rehman, *Int. J. Hydrogen. Energy* **50**, 1435 (2024).